Bromate reduction by iron(II) during managed aquifer recharge
A laboratory-scale study

Wang, Feifei; Salgado Ismodes, V.A.; van der Hoek, Jan Peter; van Halem, Doris

DOI
10.3390/w10040370

Publication date
2018

Document Version
Final published version

Published in
Water

Citation (APA)
Wang, F., Salgado Ismodes, V. A., van der Hoek, J. P., & van Halem, D. (2018). Bromate reduction by iron(II) during managed aquifer recharge: A laboratory-scale study. *Water*, *10*(4), Article 370. https://doi.org/10.3390/w10040370

water

MDPI

Article

Bromate Reduction by Iron(II) during Managed Aquifer Recharge: A Laboratory-Scale Study

Feifei Wang [1,*], Vanida Salgado [1], Jan Peter van der Hoek [1,2] and Doris van Halem [1]

[1] Department of Water Management, Faculty of Civil Engineering and Geosciences, Delft University of Technology, P.O. Box 5048, 2600 GA Delft, The Netherland; vanisalis@gmail.com (V.S.); J.P.vanderHoek@tudelft.nl (J.P.v.d.H.); D.vanHalem@tudelft.nl (D.v.H.)
[2] Strategic Centre, Waternet, Korte Ouderkerkerdijk 7, 1096 AC Amsterdam, The Netherlands
* Correspondence: f.wang-2@tudelft.nl; Tel.: +31-06-1533-9539

Received: 22 February 2018; Accepted: 22 March 2018; Published: 24 March 2018

Abstract: The removal of bromate (BrO_3^-) as a byproduct of ozonation in subsequent managed aquifer recharge (MAR) systems has so far gained little attention. This preliminary study with anoxic batch experiments was executed to explore the feasibility of chemical BrO_3^- reduction in Fe-reducing zones of MAR systems and to estimate potential inhibition by NO_3^-. Results show that the reaction rate was affected by initial Fe^{2+}/BrO_3^- ratios and by pH. The pH dropped significantly due to the hydrolysis of Fe^{3+} to hydrous ferric oxide (HFO) flocs. These HFO flocs were found to adsorb Fe^{2+}, especially at high Fe^{2+}/BrO_3^- ratios, whereas at low Fe^{2+}/BrO_3^- ratios, the mass sum loss of BrO_3^- and Br^- indicated intermediate species formation. Under MAR conditions with relatively low BrO_3^- and Fe^{2+} concentrations, BrO_3^- can be reduced by naturally occurring Fe^{2+}, as the extensive retention time in MAR systems will compensate for the slow reaction kinetics of low BrO_3^- and Fe^{2+} concentrations. Under specific flow conditions, Fe^{2+} and NO_3^- may co-occur during MAR, but NO_3^- hardly competes with BrO_3^-, since Fe^{2+} prefers BrO_3^- over NO_3^-. However, it was found that when NO_3^- concentration exceeds BrO_3^- concentration by multiple orders of magnitude, NO_3^- may slightly inhibit BrO_3^- reduction by Fe^{2+}.

Keywords: drinking water treatment; bromate reduction; ozonation; iron-reducing zones; managed aquifer recharge; nitrate

1. Introduction

Managed aquifer recharge (MAR) has proven to be an effective barrier for many organic micropollutants (OMPs) present in surface water during drinking water production [1–3]. However, some highly persistent OMPs can still be detected in MAR filtrate [4] and may reach the drinking water supply [5]. Ozone-based advanced oxidation processes (AOPs) are increasingly being considered as effective alternatives for the removal of OMPs during drinking water treatment [6–8]. The combination of MAR with ozonation as a pretreatment has been suggested as a comprehensive multibarrier treatment system to effectively remove various OMPs during drinking water production [9–11]. However, bromate (BrO_3^-) is formed during ozone-based treatment when applied to bromide-containing water [12–14]. It has been reported that the BrO_3^- concentration in drinking water after ozone-based AOPs typically ranges from 0 to 127 µg/L (1 µM) [15]. BrO_3^- is classified as Group 2B, or possible human carcinogen, by the International Agency for Research on Cancer based on its major toxic effects [16–18]. The standard of BrO_3^- in drinking water regulated by the World Health Organization, the US Environmental Protection Agency, and the European Union is 10 µg/L [19–21], demanding water companies to control the BrO_3^- concentration in drinking water.

A number of physical, chemical, electrochemical, and biological techniques for BrO_3^- removal have already been proposed. With respect to physical techniques, various advanced sorption materials, e.g., ion-exchange resins [22], nanocrystalline akaganeite (β-FeOOH)–coated quartz sand [23], and layered double hydroxides [24,25], have shown the ability to adsorb BrO_3^- from aqueous solutions, but so far these have not been applied in drinking water treatment. The use of granular activated carbon (GAC) as a conventional physical sorption technique can successfully reduce BrO_3^- [26], but the regenerated GAC loses effectiveness for BrO_3^- removal after a certain running time [15]. BrO_3^- can be removed by reverse osmosis [27], but this is an expensive process, since membrane fluxes are low and high operating pressures are needed. Electrodialysis reversal (EDR) has been studied in an integrated membrane system for drinking water treatment [28], which showed only limited BrO_3^- removal: 64% in a two-stage EDR system and 78% in a three-stage EDR system. BrO_3^- removal with catalysts, including zero-valent iron (Fe) [29] and Pd/Al_2O_3 [30], has been found to be limited in the presence of coexisting anions. Different reducing agents, such as ferrous iron ($FeSO_4$), react with dissolved oxygen (DO), and therefore their practical application during water treatment is quite difficult [31]. UV irradiation successfully reduces BrO_3^- but has a high energy demand [15], just like electrochemical methods [32,33]. With respect to biological techniques, biological activated carbon (BAC) filters are capable of reducing BrO_3^- effectively, but competitive DO remains a critical factor [34], because it is a challenge to construct a BAC filter with restricted oxygen transfer within the biofilm [35]. Hijnen et al. [36] showed that BrO_3^- was removed in a denitrifying bioreactor fed with methanol. However, they demonstrated that this did not seem to be a realistic option for drinking water treatment due to the long contact times required for BrO_3^- removal and extensive posttreatment necessary to remove excess methanol and released biomass. Altogether, there are few effective options to remove highly soluble and stable BrO_3^- in practice.

In this study, a new approach is being proposed, namely to utilize Fe-reducing zones of MAR as a barrier for BrO_3^- after ozonation. This sequence of AOP–MAR has been proposed to effectively remove various OMPs during drinking water production [9–11]. It is hypothesized that not only will the removal of OMPs improve with this sequence, but the produced BrO_3^- will be removed by MAR. Recently, it was found that BrO_3^- is partially biodegraded in NO_3^--reducing zones of MAR [37,38]. However, the potential reduction of BrO_3^- to Br^- in deeper Fe-reducing zones during soil passage has not yet been investigated.

The reduction of BrO_3^- by Fe^{2+} [31,39] and the hydrolysis of its product Fe^{3+} under near-neutral pH proceed as follows [40,41]:

$$BrO_3^- + 6\,Fe^{2+} + 6\,H^+ \rightarrow Br^- + 6\,Fe^{3+} + 3\,H_2O \tag{1}$$

$$Fe^{3+} + 3H_2O \rightarrow Fe(OH)_{3\,(s)} + 3H^+ \tag{2}$$

$$BrO_3^- + 6\,Fe^{2+} + 15\,H_2O \rightarrow Br^- + 6\,Fe(OH)_{3\,(s)} + 12\,H^+ \tag{3}$$

The reduction rate of BrO_3^- by Fe^{2+} is dependent on Fe^{2+} concentration, contact time, pH, and DO [31,42]. In MAR systems, water flows from infiltration ponds through an oxic zone, via an NO_3^--reducing anoxic zone and an Mn-reducing anoxic zone, to the Fe-reducing anoxic zone. So, depending on the local geochemical situation of MAR, Fe^{2+} may be released into the groundwater, leading to natural BrO_3^- reduction by Fe^{2+} in the Fe-reducing anoxic zone of MAR.

A study by Siddiqui et al. [31] with oxic water (0.22 mM DO) found that an initial BrO_3^- concentration of 0.4 μM was lowered to 0.08 μM within 30 minutes following a dose of 0.27 mM Fe^{2+}. Dong et al. [42] worked with 0.2 μM BrO_3^-, a 0.54 mM Fe^{2+} dosage, and 0.07 mM DO, reaching a BrO_3^- reduction of 65%. In these studies, the Fe^{2+} dosage was extremely high compared to expected Fe^{2+} concentrations during MAR, when Fe concentrations below 0.03 mM are expected (e.g., the MAR site of Dunea, the Netherlands, shows concentrations ranging from 0.0015 to 0.029 mM Fe). However, little is known about the reaction of BrO_3^- and Fe^{2+} in such low concentrations. Additionally, to what extent BrO_3^- reduction is possible at such low concentrations of Fe^{2+} is not known, although the extensive residence times in the subsurface do not require fast kinetics for this technology to be effective. Also, competition of BrO_3^- with DO is not a problem in these anoxic zones. Fe^{2+} can be formed only when NO_3^- as an electron acceptor is exhausted in anaerobic zones of MAR systems [43,44]. However, water containing NO_3^- and water containing Fe^{2+} from different pathways have been found to mix in specific zones of MAR [45], so NO_3^- and Fe^{2+} can be present simultaneously in anaerobic zones of MAR systems. This was confirmed by Dunea measurements, where NO_3^- and dissolved Fe have been detected simultaneously in the effluent of MAR sites (Scheveningen and Monster, the Netherlands). Therefore, NO_3^- may compete with BrO_3^- for reduction by Fe^{2+} [46–48] during MAR. The investigation of BrO_3^- reduction by Fe^{2+} in the presence of NO_3^- may be an important reference for the feasibility of BrO_3^- removal in Fe-reducing zones of MAR systems. Examples of stoichiometric equations for the reaction of NO_3^- and Fe^{2+} in which the stable endpoint is nitrogen gas are given below, but less complete reactions may have endpoints anywhere along the reduction pathway [49]:

$$10Fe^{2+} + 2NO_3^- + 14H_2O \rightarrow 10FeOOH + N_2 + 18H^+ \tag{4}$$

$$15Fe^{2+} + NO_3^- + 13H_2O \rightarrow 5Fe_3O_4 + N_2 + 28H^+ \tag{5}$$

The focus of this preliminary study was to investigate the mechanism of chemical BrO_3^- reduction by Fe^{2+} and the feasibility of BrO_3^- reduction by naturally occurring Fe^{2+} in the Fe-reducing anoxic zones of MAR systems, with an emphasis on the potential competition with or inhibition by NO_3^-. Microbiological reactions and biochemical reactions were not included in this study.

2. Materials and Methods

2.1. Experimental Design

The research was designed with 2 sets of anoxic batch reactor experiments: (A) high Fe^{2+} and BrO_3^- concentrations to investigate reduction mechanisms, and (B) environmentally relevant concentrations of Fe^{2+} and BrO_3^- to simulate the concentrations during MAR. As the focus in all experiments was on chemical BrO_3^- reduction by Fe^{2+}, no soil or sediment was added in the batch reactors. Both sets of experiments were executed in the absence and presence of NO_3^-. An overview of all experiments is provided in Figure 1.

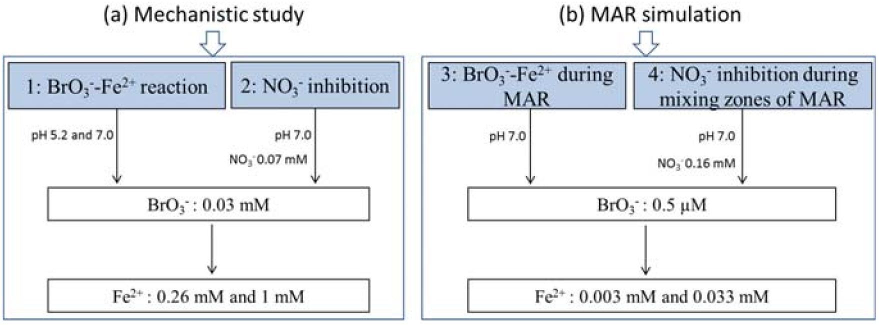

Figure 1. Experimental overview of anoxic batch reactors. T = 11.5 ± 0.5 °C ($n = 2$). MAR: managed aquifer recharge.

For the experiments with high Fe^{2+} and BrO_3^- concentrations, anoxic batch experiments were performed with 0.03 mM BrO_3^- and 0.26 or 1 mM Fe^{2+}. The concentration of 0.26 mM Fe^{2+} is close to the required concentration to reduce 0.03 mM BrO_3^- according to the stoichiometry of Equation (1). The experiments were executed under 2 pH conditions: pH 7.0, which is realistic for MAR water, and pH 5.2 to slow down the reaction in order to identify potential intermediate species.

To investigate the competition between NO_3^- and BrO_3^-, the same order of magnitude of NO_3^- (0.07 mM) and BrO_3^- (0.03 mM) was added to anoxic batch reactors, together with the Fe^{2+} (0.26 mM and 1 mM).

To simulate BrO_3^- reduction by Fe^{2+} at concentrations similar to MAR, the concentrations were lowered to 0.5 μM for BrO_3^- and 0.003–0.033 mM for Fe^{2+}. The concentration of 0.003 mM Fe^{2+} was close to the stoichiometric amount to reduce 0.5 μM BrO_3^- (Equation (1)). These experiments were conducted at an initial pH of 7.0. The influence of NO_3^- was investigated by dosing with 0.16 mM NO_3^-, which was 3 orders of magnitude greater than the concentration of BrO_3^-. Our previous study showed that the NO_3^- concentration was in the range of 10.7 ± 6 mg/L in MAR influent water [37], so in this study 10 mg/L (0.16 mM) was chosen as a relevant concentration. BrO_3^- formation at concentrations ranging from <2–293 μg/L has been reported during ozonation of natural water under normal drinking water treatment conditions [28,50–52], but in 100 investigated drinking water utilities, BrO_3^- concentration was within the range of <2–60 μg/L after ozonation of water containing 2–429 μg/L Br^- [53,54]. For this study, it was decided to investigate the upper value of this range, so 60 μg/L BrO_3^- (0.5 μM) was dosed. All experiments were performed in duplicate.

2.2. Anoxic Batch Reactors

Four series of laboratory-scale batch experiments using 250 mL (A experiments) and 1 L (B experiments) glass bottles were carried out under anoxic conditions at a controlled temperature (11.5 ± 0.5 °C). Anoxic conditions were reached by flushing nitrogen gas until a DO concentration below 0.3 μM (0.01 mg/L) was achieved in the batch reactors. The mouths of the batch reactors were sealed with rubber stoppers to prevent DO intrusion. On the rubber stoppers, there were 2 needles with valves, used as a sampling point and a reagent dosing point.

Water samples were collected 8–10 times within 120 h contact time to determine the concentrations of BrO_3^-, Br^-, NO_3^-, and Fe^{2+}. In the 0.03 mM BrO_3^- experiments (A) and 0.5 μM BrO_3^- experiments (B), 3 mL and 50 mL per sample were collected, respectively. After sample collection, several drops of diluted ethylenediamine (EDA) solution (11%) was added to the samples to prevent reactions of residual chemicals [55].

To test the stability of the anoxic system, Fe^{2+} concentrations were monitored in the batch reactors after dosing with 0.033, 0.003, 0.26, or 1 mM Fe^{2+}. The Fe^{2+} concentrations remained sFig during the 120 h experiment (Figure 2), indicating that the system was well sealed, and therefore no Fe^{2+} oxidation by DO was observed.

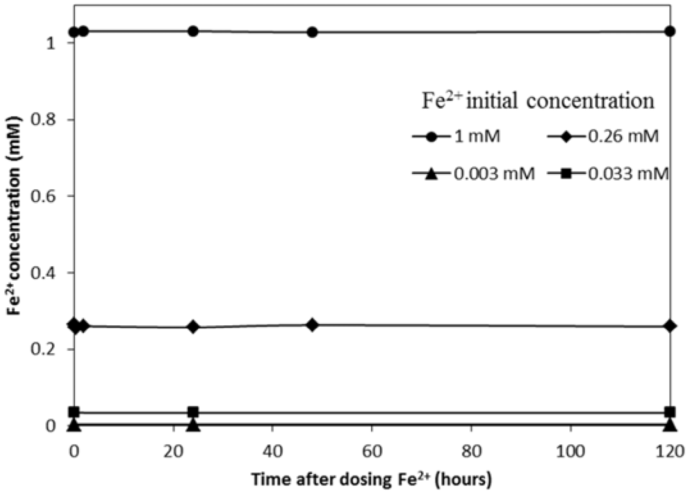

Figure 2. Fe^{2+} concentrations over 120 h contact time in reactors with Fe^{2+} alone.

2.3. Water and Chemicals

The water used in batch experiments was prepared using chemical reagents and deionized water from a Millipore Milli-Q system. Sodium bromate ($NaBrO_3$), sodium nitrate ($NaNO_3$), ferrous sulfate ($FeSO_4{\cdot}7H_2O$), sodium bicarbonate ($NaHCO_3$), and EDA were purchased from Sigma-Aldrich (St. Louis, MO, USA). The amount of 2 mM $NaHCO_3$ was prepared for use as a pH buffer, and 0.2 M NaOH was prepared to further adjust the pH. To prevent Fe^{2+} oxidation in $FeSO_4$ solutions, the solutions were always prepared immediately before the experiments and concentrated acid (HCl) was used to acidify the $FeSO_4$ solutions to pH 2 [55]. All chemicals were of analytical grade.

2.4. Analytical Methods

DO and temperature were measured with an FDO® 925 optical oxygen sensor (WTW) (Xylem Inc., Weilheim, Germany) and pH was measured with a SenTix® 940 (WTW) electrode (Xylem Inc., Weiheim, Germany), both using the WTW Multi 3420 meter (Xylem Inc., Weiheim, Germany).

Fe^{2+} was measured by photometry using the Spectroquant® iron test (Merck, Kenilworth, NJ, USA) with a detection range of 0.0002–0.09 mM. Dilution factors of 4 and 16 were needed to measure the Fe^{2+} in the experiments with dosages of 0.26 and 1 mM, respectively. For the dosages of 0.003 and 0.033 mM Fe^{2+}, no dilution was required.

The NO_3^- concentration in all experiments was determined by an ion chromatograph (Metrohm 881 Compact IC pro-Anion, Metrohm AG, Herisau, Switzerland) with an A Supp 16-150/4.0 anion column (Metrohm AG, Herisau, Switzerland). For experiments using 0.03 mM BrO_3^- (A), BrO_3^- and Br^- were measured by the same equipment as for NO_3^-. The detection limits of BrO_3^-, Br^-, and NO_3^- were 0.008 mM, 0.001 mM, and 0.002 mM, respectively. For experiments using 0.5 μM BrO_3^- (B), water samples were analyzed at Het Waterlaboratorium (Haarlem, the Netherlands), where an ion chromatograph (Dionex ICS-300, Thermo Fisher Scientific Inc., Waltham, MA, USA) with IonPac AS9SC column (250 mm × 4 mm ID, Thermo Fisher Scientific Inc., Waltham, MA, USA) was used to measure BrO_3^-. An ion chromatograph (Dionex ICS-1100, Thermo Fisher Scientific Inc., Waltham, MA, USA) with IonPac AG22 column (4 × 50 mm, Thermo Fisher Scientific Inc., Waltham, MA, USA) and IonPac AS22SC column (4 × 250 mm, Thermo Fisher Scientific Inc., Waltham, MA, USA) was used to measure Br^-. The detection limits for BrO_3^- and Br^- were 0.004 μM and 0.125 μM, respectively.

3. Results

3.1. BrO_3^- Reduction Rate and Mass Balance

Figure 3 presents the kinetics of BrO_3^- reduction and Br^- formation within 120 h after the addition of 0.26 and 1 mM Fe^{2+}. The experiments were executed at pH 5.2 and 7.0, the latter being most representative of MAR water. For BrO_3^- (0.03 mM), the 0.26 mM Fe^{2+} dosage was close to the stoichiometric ratio (1 mol BrO_3^-:6 mol Fe^{2+}) according to Equation (1). For this particular setting, >90% of initial BrO_3^- reduced into Br^- within 120 h (Figure 3a,c). The BrO_3^- reduction fit second-order reaction kinetics well. Moreover, for pH 5.2 and 7.0, the kinetic constant was 2.5 and 3.3, respectively, and the BrO_3^- reduction rate was 0.00024 μM/min and 0.00026 μM/min, respectively, indicating that pH 7 promoted BrO_3^- reduction compared to pH 5.2. In the case of the 1 mM Fe^{2+} dosage, BrO_3^- reduction was accelerated, with almost 100% BrO_3^- reduction to Br^- within 1 h at pH 5.2 (Figure 3b) and pH 7.0 (Figure 3d). These results indicate that the higher the Fe^{2+} dosage, the higher the BrO_3^- reduction rate, which is in line with existing literature [31,42].

Figure 4 shows the consumed Fe^{2+}/BrO_3^- ratios after 24, 48, and 120 h. In the case of the 1 mM Fe^{2+} dosage (corresponding to an initial ratio of $Fe^{2+}/BrO_3^- = 33$), consumed Fe^{2+}/BrO_3^- ratios were higher than the theoretical ratio of 6 according to Equation (1), which assumes a total reduction of BrO_3^- to Br^-. After 24 h, the ratios were 8.0 and 9.2 for pH 5.2 and pH 7.0, respectively, with BrO_3^- reduced to below the detection limit. Between 24 and 120 h, Fe^{2+} continued to be consumed, and correspondingly, Fe^{2+}/BrO_3^- ratios increased. This may be explained by Fe^{2+} adsorption onto hydrolyzed Fe^{3+} flocs of hydrous ferric oxide (HFO). Interestingly, there was a consumed Fe^{2+}/BrO_3^- ratio below the stoichiometric ratio of 6 in the case of the 0.26 mM Fe^{2+} dosage (corresponding initial $Fe^{2+}/BrO_3^- = 8$). The ratio below 6 could indicate the production of intermediate Br species during the reduction of BrO_3^-, requiring less Fe^{2+} compared to the total reduction of BrO_3^- to Br^- as in Equation (1). Additionally, the molar mass sum of BrO_3^- and Br^- slightly decreased during the experiment by 10–20%, indicating that intermediate products may have formed.

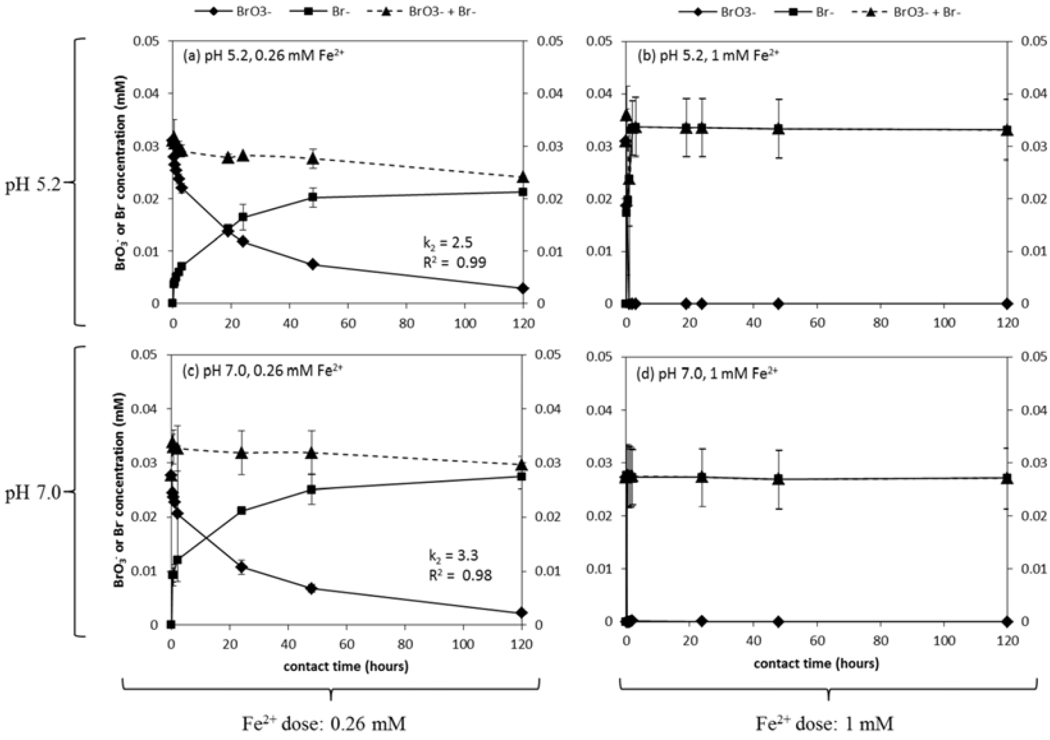

Figure 3. BrO_3^- reduction after dosing with (**a**,**c**) 0.26 mM or (**b**,**d**) 1 mM Fe^{2+}. Initial BrO_3^- concentration was 0.03 mM and initial pH levels were 5.2 and 7.0. The calculated BrO_3^- reduction rates were 0.00024 μM/min and 0.00026 μM/min for a and c.

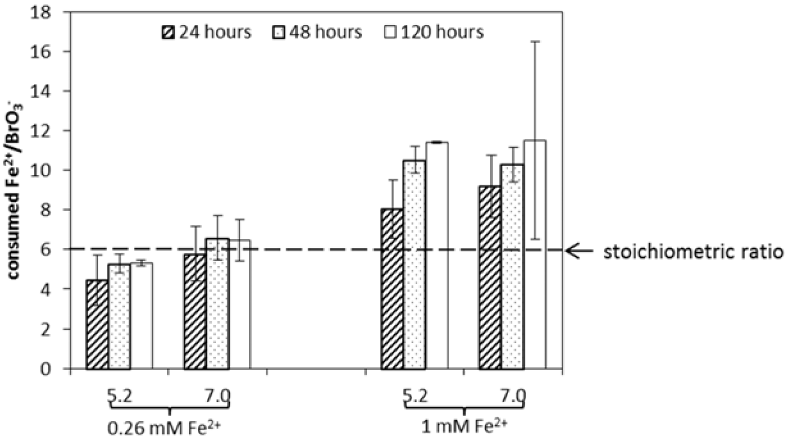

Figure 4. The consumed Fe^{2+}/BrO_3^- ratios after dosing with 0.26 mM or 1 mM Fe^{2+} to a solution containing 0.03 mM BrO_3^- at two initial pH levels, 5.2 and 7.0.

3.2. NO_3^-, *A Competing Electron Acceptor?*

NO_3^- is known to act as a competitive electron acceptor in the reaction with Fe^{2+} [48]. Figure 5 depicts BrO_3^- reduction by Fe^{2+} in the presence of NO_3^- at a concentration at the same order of magnitude as BrO_3^- (0.07 mM). The rate of BrO_3^- reduction in the presence of NO_3^- was slightly lower compared to the absence of NO_3^- (Figure 3c). NO_3^- concentrations in these experiments were steady during the 120 h for both Fe^{2+} dosages (Figure 5a,b), indicating that Fe^{2+} did not reduce NO_3^- when BrO_3^- and NO_3^- were present simultaneously.

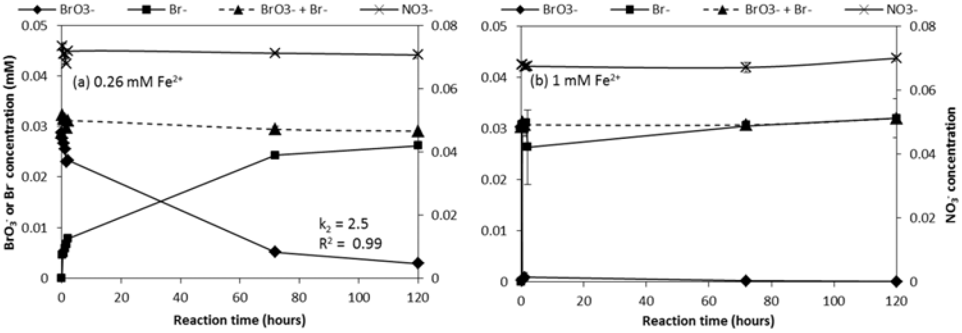

Figure 5. BrO_3^- reduction after dosing with (**a**) 0.26 mM or (**b**) 1 mM Fe^{2+} in the presence of NO_3^-. Initial BrO_3^- and NO_3^- concentrations were 0.03 mM and 0.07 mM, respectively, and initial pH was 7.0.

Figure 6 shows BrO_3^- and Fe^{2+} consumption in the presence and absence of 0.07 mM NO_3^-. BrO_3^- removal in the presence and absence of NO_3^- was the same for both Fe^{2+} dosages, while the presence of NO_3^- led to higher Fe^{2+} consumption with the 0.26 mM Fe^{2+} dosage. The additional Fe^{2+} removal (62%→71%), 0.02 mM, might have reacted with NO_3^-, but the change would have remained undetected, given that it would have resulted in a calculated reduction of <0.005 mM NO_3^- (NO_3^-/Fe^{2+} ratio, Equations (4) and (5)). This would not have been noted by our NO_3^- analytical methods. Nevertheless, based on the above results, it can be concluded that BrO_3^- reduction was hardly affected by NO_3^- presence and that Fe^{2+} preferred BrO_3^- to NO_3^- as an electron acceptor. This was also observed by Westerhoff [56], who suggested that the difference in structure (atomic radii and O-bonds) makes it relatively easier to remove an O atom from a BrO_3^- ion than a NO_3^- ion. In addition, the preference of Fe^{2+} for BrO_3^- reduction vs. NO_3^- reduction can also be attributed to the higher ΔE [57–59] of oxidation-reduction reactions:

$$Fe^{2+} \rightarrow Fe^{3+} + e,\ E_1 = -0.771\ V \tag{6}$$

$$2BrO_3^- + 12H^+ + 10e \rightarrow Br_2 + 6H_2O,\ E_2 = 1.52\ V \tag{7}$$

$$Br_2 + 2e \rightarrow 2\ Br^-,\ E_3 = 1.087\ V \tag{8}$$

$$NO_3^- + 3H^+ + 2e \rightarrow HNO_2 + H_2O,\ E_4 = 0.94\ V \tag{9}$$

$$HNO_2 + H^+ + e \rightarrow NO + H_2O,\ E_5 = 1.00\ V \tag{10}$$

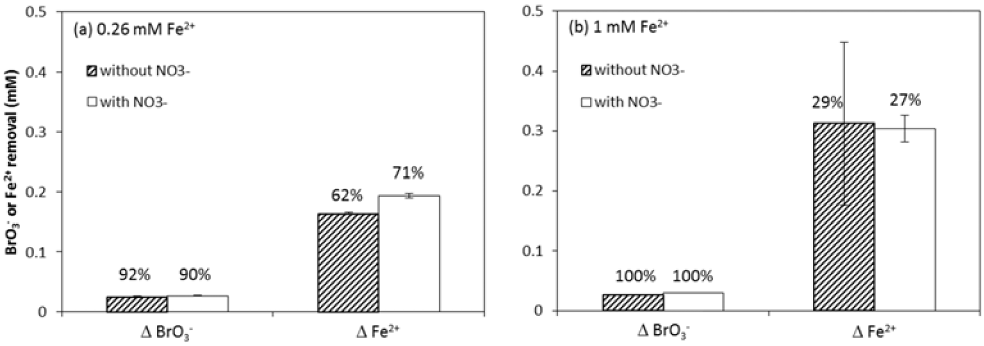

Figure 6. The effect of 0.07 mM NO_3^- on the reduction of 0.03 mM BrO_3^- 120 h after dosing with (**a**) 0.26 mM or (**b**) 1 mM Fe^{2+} at initial pH 7.0 corresponds to the removal percentages.

Reactions 6 and 7 are preferable over 6 and 9.

3.3. pH Change and Fe^{3+} Hydrolysis

Although the BrO_3^- reduction in Equation (1) shows a pH increase, reduction of BrO_3^- by Fe^{2+} consequently means that Fe^{2+} is oxidized to Fe^{3+}, and subsequently Fe^{3+} will hydrolyze to form flocs of hydrous ferric oxide (HFO) [40]. Therefore, the pH will drop based on Equation (3), the combined BrO_3^- reduction with Fe^{3+} hydrolysis. The pH drop was observed in all of the 0.03 mM BrO_3^- experiments: 1.5–1.6 drop and 2.6–3.0 drop with initial pH 5.2 and 7.0, respectively. The pH drop was an indicator of Fe^{3+} hydrolysis. Moreover, the observed yellow flocs in the batch reactors also provide evidence of HFO formation. The above two phenomena (pH decrease and visible flocs) are a strong indication that HFO flocs were formed in the reactors. The adsorption of Br^- or BrO_3^- onto HFO flocs was not expected to have occurred, as BrO_3^- and Br^- have no affinity for HFO [60]. However, Fe^{2+} adsorption onto the flocs has been frequently reported [31,61,62], which may explain the observed Fe^{2+}/BrO_3^- removal ratios beyond the stoichiometric ratio of 6 (in Figure 4).

3.4. BrO_3^- Reduction under Concentrations Similar to MAR

To investigate the rate of BrO_3^- reduction by Fe^{2+} in concentrations similar to MAR, the reduction kinetics were monitored for 0.5 μM BrO_3^- after dosing with 0.003 and 0.033 mM Fe^{2+}. Figure 7a,b show the BrO_3^- and Br^- kinetics in the absence of NO_3^-, while Figure 7c,d show the kinetics of BrO_3^- and Br^- in the presence of 0.16 mM NO_3^-. As in the previous experiments with high BrO_3^- concentrations, the reduction rate of 0.5 μM BrO_3^- also depends on the Fe^{2+} concentration, with a higher rate at a higher concentration. Figure 7a,c show that after 120 h contact time, there was limited BrO_3^- reduction (7% in the absence of NO_3^- and 12% in the presence of NO_3^-) at 0.003 mM Fe^{2+}, while Figure 7b,d show considerable BrO_3^- reduction at 0.033 mM Fe^{2+} (74% in the absence and 58% in the presence of NO_3^-). Assuming second-order reaction kinetics, it was calculated that the rate constant of BrO_3^- reduction at a higher Fe^{2+} dosage (0.033 mM) was 0.049 and 0.023 in the absence and presence of NO_3^-, respectively. Although the NO_3^- concentration was three orders of magnitude higher than the BrO_3^- concentration, the NO_3^- concentration was steady (Figure 7c,d). It is noteworthy that during these experiments the molar mass sum of BrO_3^- and Br^- also slightly decreased from 0.50 μM to 0.48 μM and 0.46 μM for 0.003 mM and 0.033 mM Fe^{2+} dosages, respectively, indicating the formation of Br intermediate species.

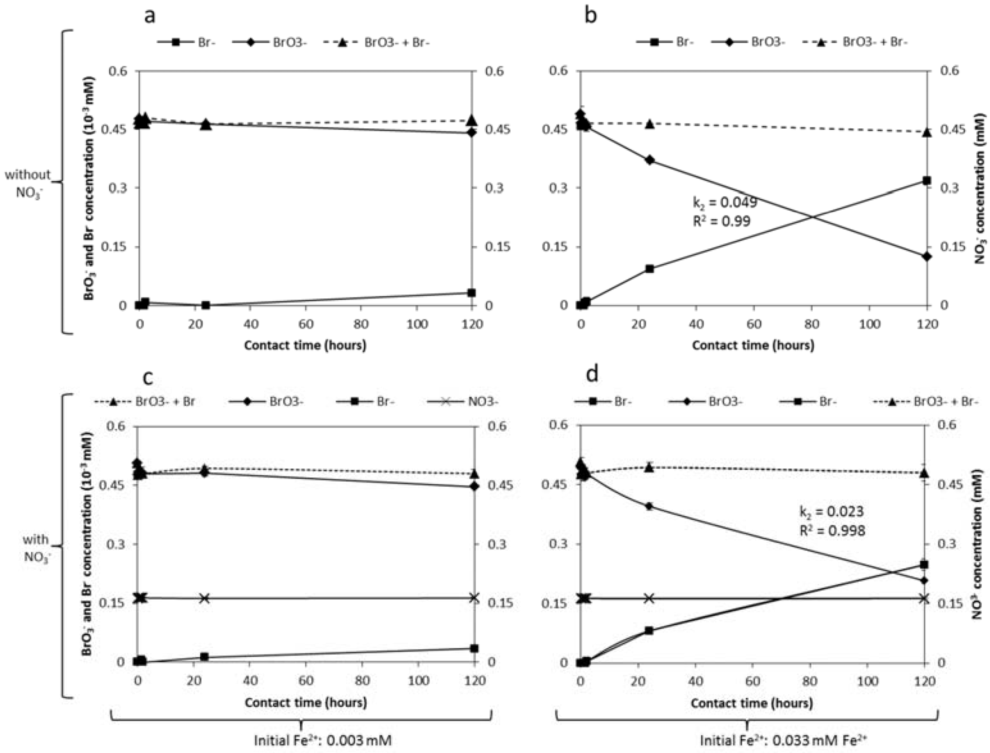

Figure 7. BrO_3^- reduction after dosing with (**a**,**c**) 0.003 mM or (**b**,**d**) 0.033 mM Fe^{2+}, simulating MAR concentrations, in the (**a**,**b**) presence and (**c**,**d**) absence of NO_3^-. (**c**,**d**) Initial BrO_3^- and NO_3^- concentrations were 0.5 µM and 0.16 mM, respectively. Initial pH was 7.0.

Figure 8 shows reduction of BrO_3^- and consumption of Fe^{2+} in the presence and absence of 0.16 mM NO_3^-. In the case of the 0.003 mM Fe^{2+} dosage, it appears that the presence of NO_3^- did not influence BrO_3^- reduction and Fe^{2+} oxidation (Figure 8a). In the case of the 0.033 mM Fe^{2+} dosage, the presence of NO_3^- led to lower BrO_3^- reduction and lower Fe^{2+} oxidation (Figure 8b). Combining the results in Figures 7 and 8 indicates that Fe^{2+} preferred BrO_3^- to NO_3^- as an electron acceptor, but it did inhibit BrO_3^- reduction to some extent. This could possibly have been set off by considerably higher NO_3^- concentrations compared to BrO_3^-, in combination with the stoichiometric excess of Fe^{2+}. One potential reason to explain the inhibition by NO_3^- is the hypothesized formation of NO from NO_3^- complexed with Fe^{2+} [63], slowing down the reduction of BrO_3^-.

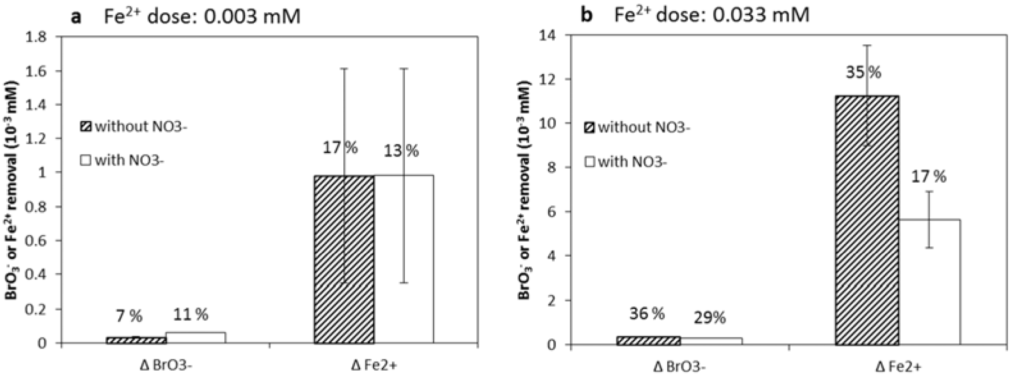

Figure 8. Consumed BrO_3^- and Fe^{2+} 120 h after dosing with (**a**) 0.003 mM or (**b**) 0.033 mM Fe^{2+} in the presence and absence of NO_3^- at initial pH 7.0. Initial BrO_3^- and NO_3^- concentrations were 0.5 µM and 0.16 mM, respectively. % corresponds to the removal percentages.

4. Discussion

4.1. BrO_3^- Reduction Mechanism

Figure 9a shows a summary of the mole sum of BrO_3^- and Br^- in all of the experiments with an initial dosage of 0.03 mM BrO_3^-. No Br mass loss was observed in the case of a sufficiently high initial Fe^{2+}/BrO_3^- ratio (33), while the mole sum of BrO_3^- and Br^- was 78–90% of the initial Br in the case of lower stoichiometric Fe^{2+}/BrO_3^- ratios (8). It is possible that Br intermediate species formed during the reduction of BrO_3^-. Equations (11)–(13) show the reduction pathways of BrO_3^- to intermediate species requiring less Fe^{2+}, as reported by Shen et al. (2017) and Siddiqui et al. (1994):

$$BrO_3^- + 2Fe^{2+} + 2H^+ \rightarrow 2Fe^{3+} + BrO_2^- + H_2O \tag{11}$$

$$BrO_2^- + 2Fe^{2+} + 2H^+ \rightarrow 2Fe^{3+} + BrO^- + H_2O \tag{12}$$

$$BrO^- + 2Fe^{2+} + 2H^+ \rightarrow 2Fe^{3+} + Br^- + H_2O \tag{13}$$

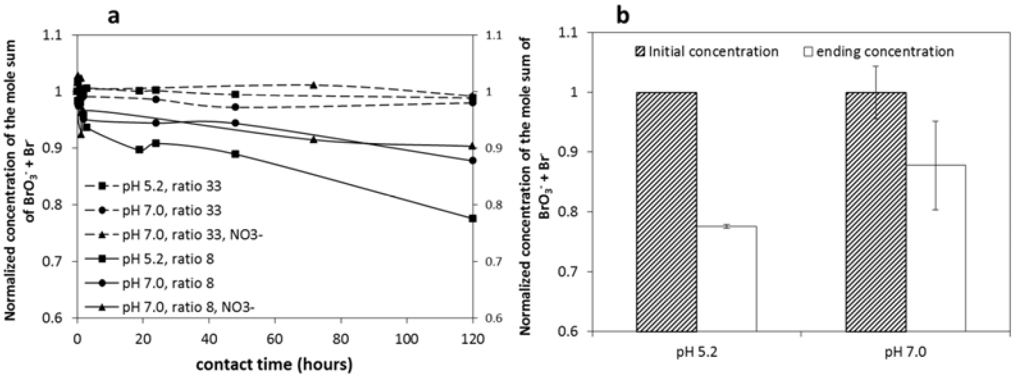

Figure 9. (**a**) Mole mass sum of BrO_3^- and Br^- in all experiments with initial BrO_3^- concentration of 0.03 mM and (**b**) comparison of mole mass loss of BrO_3^- and Br^- in 120 h between pH 5.2 and pH 7.0. Ratio means the initial ratio of Fe^{2+}/BrO_3^- ($n = 2$).

The most frequently reported intermediate species is hypobromous acid ($HOBr/BrO^-$) [31,64]. Furthermore, the study of Shen et al. [60] showed that the sum of BrO_3^-, $HBrO/BrO^-$, and Br^- was 98–101% of the initial Br (as BrO_3^-) concentration, and therefore almost no other intermediate species except for $HOBr/BrO^-$ existed. Taken together, BrO_3^- was reduced into the end product Br^- most likely via the intermediate species HBrO/BrO during the reaction of BrO_3^- and Fe^{2+} in this study.

Figure 9b shows the mole sum change of BrO_3^- and Br^- in the case of an initial Fe^{2+}/BrO_3^- ratio of 8 at pH 5.2 and 7.0. More Br loss was observed at pH 5.2 (22%) than at pH 7.0 (12%). Based on the total reaction (Equation (3)), pH 5.2 would slow down the BrO_3^- reduction, providing the intermediate species with a longer lifetime and thus a better chance to be detected in this experiment. Moreover, the intermediate species formation requires less Fe^{2+}, as shown in Equations (11)–(13). This may be one possible reason for the observation in Figure 4: a relatively low consumed Fe^{2+}/BrO_3^- ratio at pH 5.2 compared to pH 7.0. However, the lower ratio for pH 5.2 can also be partially explained by the decreased sorption of Fe^{2+} onto precipitating HFO in this experiment, while the higher Fe^{2+}/BrO_3^- ratio for pH 7.0 correlates with promoted Fe^{2+} sorption at higher pH [61]. The lower Fe^{2+}/BrO_3^- ratio at pH 5.2 compared to pH 7.0 in Figure 4 may also be related to the surface charge density. It has been reported that the lower the pH of FeOOH formation, the higher the positive surface charge density [65]. So, at pH 5.2, the formed FeOOH presents high positive charge density, potentially promoting BrO_3^- adsorption and Fe^{2+} rejection, which in turn may explain the lower Fe^{2+}/BrO_3^- ratio.

In contrast, at pH 7, the neutral to positively charged surface of FeOOH will favor Fe^{2+} adsorption and BrO_3^- rejection.

4.2. Feasibility of BrO_3^- Reduction by Fe^{2+} during MAR

Based on the results in Sections 3.1 and 3.1, a preliminary conclusion can be drawn that under anoxic conditions and at a sufficiently high Fe^{2+}/BrO_3^- ratio, chemical BrO_3^- reduction can be achieved. In MAR systems, Fe^{2+} concentrations tend to be 10^{-3} to 10^{-2} mM. Fortunately, the same is the case for BrO_3^- production after ozone-based AOPs, where concentrations are generally limited to 10^{-5} to 10^{-4} mM [16,66]. Fe^{2+} concentrations detected in Dunea MAR effluent range from 0.0015–0.029 mM, so the Fe^{2+}/BrO_3^- ratios in MAR systems are sufficiently high (15–2900). From a drinking water production perspective, the extremely slow BrO_3^- reduction shown in Section 3.4 might seem to be a very inefficient process, since treatment technologies most often have contact times of minutes. However, MAR residence times in the subsurface are weeks to months [67,68], making this process a very viable BrO_3^- removal pathway. Assuming that Fe^{2+} and BrO_3^- concentrations in Fe-reducing anoxic zones and BrO_3^- reduction follow second-order kinetics, as in Figure 7b (k_2 = 0.049), the required time to reduce BrO_3^- below the drinking water guideline of 10 μg/L (0.08 μM) is on the order of 10–20 days.

As stated previously, the theoretical sequence of MAR infiltration zones follows the sequence of oxic-NO_3^--reducing-Mn-reducing-Fe-reducing-SO_4^{2-}-reducing [69], but the possible practical cross of different flowlines may result in the joint presence of NO_3^- and Fe^{2+}. The results in Figure 7 indicate a small negative effect of NO_3^- as an inhibitor for BrO_3^- reduction by Fe^{2+}, though at sufficiently high Fe^{2+} concentrations, bromate reduction is still not inhibited. Although NO_3^- reduction by Fe^{2+} is thermodynamically not feasible, in the presence of catalysts this reaction may occur [70]. A previous study reported that the presence of Ni^{2+}, Cu^{2+}, and Ag^{2+} promoted the reaction of Fe^{2+} with NO_3^- [48]. Given the presence of these elements in nature (for example, the concentration of Cu^{2+} at Dunea's MAR site is 10^{-2} mM), these may well set off NO_3^- reduction by Fe^{2+}. Moreover, previous studies [71–73] reported NO_3^--dependent Fe^{2+} oxidation mediated by anaerobic ammonium oxidation bacteria, *Escherichia coli*, and NO_3^--reducing bacteria. Therefore, a microbial mediated kinetic reaction of Fe^{2+} and NO_3^- could also occur, leading to competition for BrO_3^- reduction in these mixing flow paths in MAR systems.

Altogether, this study has shown that chemical BrO_3^- reduction by Fe^{2+} is expected to occur in Fe-reducing anoxic zones during MAR and that NO_3^- on its own is not a strong inhibitor or competitor; nevertheless, the complexity of subsurface processes may still set off conditions where NO_3^- reduction is favored over BrO_3^-. Therefore, a subsequent study to investigate BrO_3^- reduction in simulated Fe-reducing zones, such as a column study, is highly recommended, also to include microbiological and biochemical processes that take place during MAR.

5. Conclusions

Based on anoxic batch experiments, it is concluded that BrO_3^- is readily reduced by Fe^{2+}. The reaction rate was influenced by the initial Fe^{2+}/BrO_3^- ratio and by the initial pH, i.e., a higher Fe^{2+} concentration and higher pH accelerated the reaction. The pH dropped considerably during the experiments, set off by the hydrolysis of Fe^{3+} to HFO flocs. These HFO flocs were found to adsorb Fe^{2+}, particularly at high Fe^{2+}/BrO_3^- ratios, whereas at low Fe^{2+}/BrO_3^- ratios the incomplete BrO_3^-–Br^- mass balance indicated formation of intermediate species. Overall, it can be concluded that the chemical reduction of BrO_3^- by naturally occurring Fe^{2+} during MAR can occur, as extensive retention times in the subsurface will compensate for the slow reaction kinetics of low BrO_3^- and Fe^{2+} concentrations. In the specific case that Fe^{2+}-containing and NO_3^--containing water crosses flow paths during MAR, the presence of NO_3^- will not compete with BrO_3^-, as Fe^{2+} is preferred over NO_3^- as an electron acceptor. However, it was found that the presence of NO_3^- may somewhat inhibit BrO_3^- reduction when NO_3^- concentrations are far higher than BrO_3^- concentrations. The findings in this study show that application of MAR following ozone-based AOPs broadens the application of ozone-based AOPs, as MAR removes the byproduct BrO_3^-.

Acknowledgments: The research was funded by the Dunea drinking water company and by the Top Sector TKI Water Technology Program of the Dutch Ministry of Economic Affairs (No. 2013TUD001). The authors thank Katie Friedman for English editing and the China Scholarship Council for supporting our work (201206140009).

Author Contributions: Doris van Halem, Jan Peter van der Hoek, Feifei Wang, and Vanida Salgado conceived and designed the experiments; Vanida Salgado and Feifei Wang performed the experiments; Feifei Wang and Vanida Salgado analyzed the data; Vanida Salgado and Feifei Wang contributed reagents/materials/analysis tools; Feifei Wang, Vanida Salgado, Jan Peter van der Hoek, and Doris van Halem wrote the paper.

Conflicts of Interest: The authors declare no conflict of interest. The founding sponsors had no role in the design of the study; in the collection, analysis, or interpretation of data; in the writing of the manuscript, or in the decision to publish the results.

References

1. Laws, B.V.; Dickenson, E.R.V.; Johnson, T.A.; Snyder, S.A.; Drewes, J.E. Attenuation of contaminants of emerging concern during surface-spreading aquifer recharge. *Sci. Total Environ.* **2011**, *409*, 1087–1094. [CrossRef] [PubMed]
2. Kim, H.C.; Noh, J.H.; Chae, S.R.; Choi, J.; Lee, Y.; Maeng, S.K. A multi-parametric approach assessing microbial viability and organic matter characteristics during managed aquifer recharge. *Sci. Total Environ.* **2015**, *524–525*, 290–299. [CrossRef] [PubMed]
3. Postigo, C.; Barceló, D. Synthetic organic compounds and their transformation products in groundwater: Occurrence, fate and mitigation. *Sci. Total Environ.* **2015**, *503–504*, 32–47. [CrossRef] [PubMed]
4. Drewes, J.E.; Heberer, T.; Rauch, T.; Reddersen, K. Fate of pharmaceuticals during ground water recharge. *Ground Water Monit. Remediat.* **2003**, *23*, 64–72. [CrossRef]
5. Ternes, T.A.; Meisenheimer, M.; McDowell, D.; Sacher, F.; Brauch, H.J.; Haist-Gulde, B.; Preuss, G.; Wilme, U.; Zulei-Seibert, N. Removal of pharmaceuticals during drinking water treatment. *Environ. Sci. Technol.* **2002**, *36*, 3855–3863. [CrossRef] [PubMed]
6. Hübner, U.; Miehe, U.; Jekel, M. Optimized removal of dissolved organic carbon and trace organic contaminants during combined ozonation and artificial groundwater recharge. *Water Res.* **2012**, *46*, 6059–6068. [CrossRef] [PubMed]
7. Hollender, J.; Zimmermann, S.G.; Koepke, S.; Krauss, M.; McArdell, C.S.; Ort, C.; Singer, H.; von Gunten, U.; Siegrist, H. Elimination of organic micropollutants in a municipal wastewater treatment plant upgraded with a full-scale post-ozonation followed by sand filtration. *Environ. Sci. Technol.* **2009**, *43*, 7862–7869. [CrossRef] [PubMed]
8. Scheideler, J.; Lekkerkerker-Teunissen, K.; Knol, T.; Ried, A.; Verberk, J.; van Dijk, H. Combination of O_3/H_2O_2 and uv for multiple barrier micropollutant treatment and bromate formation control—An economic attractive option. *Water Pract. Technol.* **2011**, *6*. [CrossRef]
9. Lekkerkerker, K.; Scheideler, J.; Maeng, S.K.; Ried, A.; Verberk, J.Q.J.C.; Knol, A.H.; Amy, G.; van Dijk, J.C. Advanced oxidation and artificial recharge: A synergistic hybrid system for removal of organic micropollutants. *Water Sci. Technol. Water Supply* **2009**, *9*, 643–651. [CrossRef]
10. Lekkerkerker-Teunissen, K.; Chekol, E.T.; Maeng, S.K.; Ghebremichael, K.; Houtman, C.J.; Verliefde, A.R.D.; Verberk, J.Q.J.C.; Amy, G.L.; van Dijk, J.C. Pharmaceutical removal during managed aquifer recharge with pretreatment by advanced oxidation. *Water Sci. Technol. Water Supply* **2012**, *12*, 755–767. [CrossRef]
11. Oller, I.; Malato, S.; Sánchez-Pérez, J.A. Combination of Advanced Oxidation Processes and biological treatments for wastewater decontamination—A review. *Sci. Total Environ.* **2011**, *409*, 4141–4166. [CrossRef] [PubMed]
12. Kurokawa, Y.; Maekawa, A.; Takahashi, M.; Hayashi, Y. Toxicity and carcinogenicity of potassium bromate—A new renal carcinogen. *Environ. Health Perspect.* **1990**, *87*, 309–335. [PubMed]
13. Haag, W.R.; Holgne, J. Ozonation of bromide-containing waters: Kinetics of formation of hypobromous acid and bromate. *Environ. Sci. Technol.* **1983**, *17*, 261–267. [CrossRef]

14. Assuncao, A.; Martins, M.; Silva, G.; Lucas, H.; Coelho, M.R.; Costa, M.C. Bromate removal by anaerobic bacterial community: Mechanism and phylogenetic characterization. *J. Hazard. Mater.* **2011**, *197*, 237–243. [CrossRef] [PubMed]
15. Xie, L.; Shang, C. A review on bromate occurrence and removal strategies in water supply. *Water Sci. Technol. Water Supply* **2006**, *6*, 131–136. [CrossRef]
16. Xiao, Q.; Yu, S.; Li, L.; Wang, T.; Liao, X.; Ye, Y. An overview of advanced reduction processes for bromate removal from drinking water: Reducing agents, activation methods, applications and mechanisms. *J. Hazard. Mater.* **2017**, *324*, 230–240. [CrossRef] [PubMed]
17. Kurokawa, Y.; Aoki, S.; Matsushima, Y.; Takamura, N.; Imazawa, T.; Hayashi, Y. Dose-response studies on the carcinogenicity of potassium bromate in F344 rats after long-term oral administration. *J. Natl. Cancer Inst.* **1986**, *77*, 977–982. [PubMed]
18. Crofton, K.M. Bromate: Concern for developmental neurotoxicity? *Toxicology* **2006**, *221*, 212–216. [CrossRef] [PubMed]
19. WHO. *Guidelines for Drinking-Water Quality*; World Health Organization: Geneva, Switzerland, 2011; Volume 216, pp. 303–304.
20. U.S. EPA. *Guidelines for Carcinogen Risk Assessment*; Risk Assessment Forum: Washington, DC, USA, 2005.
21. Carney, M. European drinking water standards. *J. Am. Water Works Assoc.* **1991**, *83*, 48–55. [CrossRef]
22. Chen, R.; Yang, Q.; Zhong, Y.; Li, X.; Liu, Y.; Li, X.M.; Du, W.X.; Zeng, G.M. Sorption of trace levels of bromate by macroporous strong base anion exchange resin: Influencing factors, equilibrium isotherms and thermodynamic studies. *Desalination* **2014**, *344*, 306–312. [CrossRef]
23. Xu, C.; Shi, J.; Zhou, W.; Gao, B.; Yue, Q.; Wang, X. Bromate removal from aqueous solutions by nano crystalline akaganeite (β-FeOOH)-coated quartz sand (CACQS). *Chem. Eng. J.* **2012**, *187*, 63–68. [CrossRef]
24. Zhang, Y.; Li, X. Preparation of Zn-Al CLDH to remove bromate from drinking water. *J. Environ. Eng. (USA)* **2014**, *140*. [CrossRef]
25. Theiss, F.L.; Couperthwaite, S.J.; Ayoko, G.A.; Frost, R.L. A review of the removal of anions and oxyanions of the halogen elements from aqueous solution by layered double hydroxides. *J. Coll. Interface Sci.* **2014**, *417*, 356–368. [CrossRef] [PubMed]
26. Du, X.; Yu, S.; Tang, Y. Adsorptive characteristics of bromate from aqueous solutions by modified granular activated carbon. *Huanjing Kexue Xuebao/Acta Sci. Circumstantiae* **2014**, *34*, 630–637.
27. Gyparakis, S.; Diamadopoulos, E. Formation and reverse osmosis removal of bromate ions during ozonation of groundwater in coastal areas. *Sep. Sci. Technol.* **2007**, *42*, 1465–1476. [CrossRef]
28. Van Der Hoek, J.P.; Rijnbende, D.O.; Lokin, C.J.A.; Bonné, P.A.C.; Loonen, M.T.; Hofman, J.A.M.H. Electrodialysis as an alternative for reverse osmosis in an integrated membrane system. *Desalination* **1998**, *117*, 159–172. [CrossRef]
29. Wang, Q.; Snyder, S.; Kim, J.; Choi, H. Aqueous ethanol modified nanoscale zerovalent iron in Bromate reduction: Synthesis, characterization, and reactivity. *Environ. Sci. Technol.* **2009**, *43*, 3292–3299. [CrossRef] [PubMed]
30. Chen, H.; Xu, Z.; Wan, H.; Zheng, J.; Yin, D.; Zheng, S. Aqueous bromate reduction by catalytic hydrogenation over Pd/Al_2O_3 catalysts. *Appl. Catal. B Environ.* **2010**, *96*, 307–313. [CrossRef]
31. Siddiqui, M.; Amy, G.; Ozekin, K.; Zhai, W.; Westerhoff, P. Alternative strategies for removing bromate. *J. Am. Water Works Assoc. (USA)* **1994**, *86*, 81–96. [CrossRef]
32. Kishimoto, N.; Matsuda, N. Bromate ion removal by electrochemical reduction using an activated carbon felt electrode. *Environ. Sci. Technol.* **2009**, *43*, 2054–2059. [CrossRef] [PubMed]
33. Mao, R.; Zhao, X.; Qu, J. Electrochemical Reduction of Bromate by a Pd Modified Carbon Fiber Electrode: Kinetics and Mechanism. *Electrochim. Acta* **2014**, *132*, 151–157. [CrossRef]
34. Kirisits, M.J.; Snoeyink, V.L.; Inan, H.; Chee-sanford, J.C.; Raskin, L.; Brown, J.C. Water quality factors affecting bromate reduction in biologically active carbon filters. *Water Res.* **2001**, *35*, 891–900. [CrossRef]
35. Liu, J.; Yu, J.; Li, D.; Zhang, Y.; Yang, M. Reduction of bromate in a biological activated carbon filter under high bulk dissolved oxygen conditions and characterization of bromate-reducing isolates. *Biochem. Eng. J.* **2012**, *65*, 44–50. [CrossRef]
36. Hijnen, W.A.M.; Jong, R.; van der Kooij, D. Bromate removal in a denitrifying bioreactor used in water treatment. *Water Res.* **1999**, *33*, 1049–1053. [CrossRef]

37. Wang, F.; van Halem, D.; Ding, L.; Bai, Y.; Lekkerkerker-Teunissen, K.; van der Hoek, J.P. Effective removal of bromate in nitrate-reducing anoxic zones during managed aquifer recharge for drinking water treatment. *Water Res.* **2018**, *130*, 88–97. [CrossRef] [PubMed]
38. Hübner, U.; Kuhnt, S.; Jekel, M.; Drewes, J.E. Fate of bulk organic carbon and bromate during indirect water reuse involving ozone and subsequent aquifer recharge. *J. Water Reuse Desal.* **2016**, *6*, 413–420. [CrossRef]
39. Xie, L.; Shang, C. The effects of operational parameters and common anions on the reactivity of zero-valent iron in bromate reduction. *Chemosphere* **2007**, *66*, 1652–1659. [CrossRef] [PubMed]
40. Stefánsson, A. Iron(III) hydrolysis and solubility at 25 °C. *Environ. Sci. Technol.* **2007**, *41*, 6117–6123. [CrossRef] [PubMed]
41. Appelo, C.A.J.; Postma, D. *Geochemistry, Groundwater and Pollution*; CRC Press: Boca Raton, FL, USA, 2004.
42. Dong, Z.J.; Dong, W.Y.; Zhang, X.M.; Yu, X.H.; Ou, Y.F.; Du, H. Removal of bromate by ferrous sulfate reduction in drinking water. In Proceedings of the 2009 3rd International Conference on Bioinformatics and Biomedical Engineering (iCBBE), Beijing, China, 11–13 June 2009.
43. Barbieri, M.; Carrera, J.; Sanchez-Vila, X.; Ayora, C.; Cama, J.; Köck-Schulmeyer, M.; de Alda, M.L.; Barceló, D.; Brunet, J.T.; García, M.H. Microcosm experiments to control anaerobic redox conditions when studying the fate of organic micropollutants in aquifer material. *J. Contam. Hydrol.* **2011**, *126*, 330–345. [CrossRef] [PubMed]
44. Kedziorek, M.A.M.; Geoffriau, S.; Bourg, A.C.M. Organic matter and modeling redox reactions during river bank filtration in an alluvial aquifer of the Lot River, France. *Environ. Sci. Technol.* **2008**, *42*, 2793–2798. [CrossRef] [PubMed]
45. Grischek, T.; Paufler, S. Prediction of iron release during riverbank filtration. *Water* **2017**, *9*, 317. [CrossRef]
46. Song, X.; Wang, S.; Wang, Y.; Zhao, Z.; Yan, D. Addition of Fe^{2+} increase nitrate removal in vertical subsurface flow constructed wetlands. *Ecol. Eng.* **2016**, *91*, 487–494. [CrossRef]
47. Huang, Y.H.; Zhang, T.C. Effects of low pH on nitrate reduction by iron powder. *Water Res.* **2004**, *38*, 2631–2642. [CrossRef] [PubMed]
48. Buresh, R.J.; Moraghan, J. Chemical reduction of nitrate by ferrous iron. *J. Environ. Qual.* **1976**, *5*, 320–325. [CrossRef]
49. Ottley, C.J.; Davison, W.; Edmunds, M.W. Chemical catalysis of nitrate reduction by iron (II). *Geochim. Cosmochim. Acta* **1997**, *61*, 1819–1828. [CrossRef]
50. Krasner, S.W.; Glaze, W.H.; Weinberg, H.S.; Daniel, P.A.; Najm, I.N. Formation and control of bromate during ozonation of waters containing bromide. *J. Am. Water Works Assoc.* **1993**, *85*, 73–81. [CrossRef]
51. Glaze, W.H.; Weinberg, H.S.; Cavanagh, J.E. Evaluating the formation of brominated DBPs during ozonation. *J. Am. Water Works Assoc.* **1993**, *85*, 96–103. [CrossRef]
52. Amy, G.; Bull, R.; Craun, G.F.; Pegram, R.; Siddiqui, M. *Disinfectants and Disinfectant by-Products*; World Health Organization: Geneva, Switzerland, 2000.
53. Butler, R.; Godley, A.; Lytton, L.; Cartmell, E. Bromate environmental contamination: Review of impact and possible treatment. *Crit. Rev. Environ. Sci. Technol.* **2005**, *35*, 193–217. [CrossRef]
54. Kirisits, M.J.; Snoeyink, V.L. Reduction of bromate in a BAC filter. *J. Am. Water Works Assoc.* **1999**, *91*, 74–84. [CrossRef]
55. Thomas, D.; Rohrer, J. *Determination of Chlorite, Bromate, Bromide, and Chlorate in Drinking Water by Ion Chromatography with an On-Line-Generated Postcolumn Reagent for Sub-μg/L Bromate Analysis*; Thermo Fisher Scientific: Sunnyvale, CA, USA, 2017.
56. Westerhoff, P. Reduction of nitrate, bromate, and chlorate by zero valent iron (Fe^0). *J. Environ. Eng.* **2003**, *129*, 10–16. [CrossRef]
57. Lengyel, I.; Nagy, I.; Bazsa, G. Kinetic study of the autocatalytic nitric acid-bromide reaction and its reverse, the nitrous acid-bromine reaction. *J.Phys. Chem.* **1989**, *93*, 2801–2807. [CrossRef]
58. Britton, H.; Britton, H.G. 746. A potentiometric study of the reduction by potassium iodide of potassium bromate in sulphuric and hydrochloric acid solutions. *J. Chem. Soc. (Resumed)* **1952**, 3887–3892. [CrossRef]
59. Aksut, A. Investigation of Fe^{3+}/Fe^{2+} redox reaction by electrochemical methods in aqueous solution. *Commun. Fac. Sci. Univ. Ank. Ser. B* **1994**, *40*, 83–93.
60. Shen, W.; Lin, F.; Jiang, X.; Li, H.; Ai, Z.; Zhang, L. Efficient removal of bromate with core-shell $Fe@Fe_2O_3$ nanowires. *Chem. Eng. J.* **2017**, *308*, 880–888. [CrossRef]

61. Hiemstra, T.; van Riemsdijk, W.H. Adsorption and surface oxidation of Fe(II) on metal (hydr)oxides. *Geochim. Cosmochim. Acta* **2007**, *71*, 5913–5933. [CrossRef]
62. Williams, A.G.B.; Scherer, M.M. Spectroscopic evidence for Fe(II)-Fe(III) electron transfer at the iron oxide-water interface. *Environ. Sci. Technol.* **2004**, *38*, 4782–4790. [CrossRef] [PubMed]
63. Baldwin, S.A.; van Weert, G. On the catalysis of ferrous sulphate oxidation in autoclaves by nitrates and nitrites. *Hydrometallurgy* **1996**, *42*, 209–219. [CrossRef]
64. Ohura, H.; Imato, T.; Kameda, K.; Yamasaki, S. Potentiometric determination of bromate using an Fe(III)-Fe(II) potential buffer by circulatory flow-injection analysis. *Anal. Sci.* **2004**, *20*, 513–518. [CrossRef] [PubMed]
65. Tresintsi, S.; Simeonidis, K.; Vourlias, G.; Stavropoulos, G.; Mitrakas, M. Kilogram-scale synthesis of iron oxy-hydroxides with improved arsenic removal capacity: Study of Fe (II) oxidation–precipitation parameters. *Water Res.* **2012**, *46*, 5255–5267. [CrossRef] [PubMed]
66. Wang, F.; van Halem, D.; van der Hoek, J.P. The fate of H_2O_2 during managed aquifer recharge: A residual from advanced oxidation processes for drinking water production. *Chemosphere* **2016**, *148*, 263–269. [CrossRef] [PubMed]
67. Wang, F.; van Halem, D.; Liu, G.; Lekkerkerker-Teunissen, K.; van der Hoek, J.P. Effect of residual H_2O_2 from advanced oxidation processes on subsequent biological water treatment: A laboratory batch study. *Chemosphere* **2017**, *185*, 637–646. [CrossRef] [PubMed]
68. Maeng, S.K.; Sharma, S.K.; Lekkerkerker-Teunissen, K.; Amy, G.L. Occurrence and fate of bulk organic matter and pharmaceutically active compounds in managed aquifer recharge: A review. *Water Res.* **2011**, *45*, 3015–3033. [CrossRef] [PubMed]
69. Stuyfzand, P.J. Hydrology and water quality aspects of Rhine bank groundwater in The Netherlands. *J. Hydrol.* **1989**, *106*, 341–363. [CrossRef]
70. Eckert, P.; Appelo, C.A.J. Hydrogeochemical modeling of enhanced benzene, toluene, ethylbenzene, xylene (BTEX) remediation with nitrate. *Water Resour. Res.* **2002**, *38*. [CrossRef]
71. Benz, M.; Brune, A.; Schink, B. Anaerobic and aerobic oxidation of ferrous iron at neutral pH by chemoheterotrophic nitrate-reducing bacteria. *Arch. Microbiol.* **1998**, *169*, 159–165. [CrossRef] [PubMed]
72. Oshiki, M.; Ishii, S.; Yoshida, K.; Fujii, N.; Ishiguro, M.; Satoh, H.; Okabe, S. Nitrate-dependent ferrous iron oxidation by anaerobic ammonium oxidation (anammox) bacteria. *Appl. Environ. Microbiol.* **2013**, *79*, 4087–4093. [CrossRef] [PubMed]
73. Brons, H.J.; Hagen, W.R.; Zehnder, A.J.B. Ferrous iron dependent nitric oxide production in nitrate reducing cultures of *Escherichia coli*. *Arch. Microbiol.* **1991**, *155*, 341–347. [CrossRef] [PubMed]